Ultrafast oscilloscope based on laser-triggered field emitters

Catherine Kealhofer,[1,*] Brannon B. Klopfer,[2] Gunnar E. Skulason,[3] Thomas Juffmann,[3] Seth M. Foreman,[4] and Mark A. Kasevich[2,3]

[1]*Max Planck Institute of Quantum Optics and Ludwig-Maximilians-Universität München, Am Coulombwall 1, 85748 Garching, Germany*

[2]*Applied Physics Department, Stanford University, Stanford, California 94305, USA*

[3]*Physics Department, Stanford University, Stanford, California 94305, USA*

[4]*Department of Physics and Astronomy, University of San Francisco, 2130 Fulton St., San Francisco, California 94117, USA*

**Corresponding author: C.Kealhofer@physik.uni-muenchen.de*

Received November 5, 2014; accepted November 30, 2014;
posted December 16, 2014 (Doc. ID 225953); published January 14, 2015

Laser-triggered electron emission from sharp metal tips has been demonstrated in recent years as a high brightness, ultrafast electron source. Its possible applications range from ultrafast electron microscopy to laser-based particle accelerators to electron interferometry. The ultrafast nature of the emission process allows for the sampling of an instantaneous radio frequency (RF) voltage that has been applied to a field emitter. For proof-of-concept, we use an RF signal derived from our laser's repetition rate, mapping a 9.28 GHz signal in 22.4 fs steps with 28 mv accuracy. © 2015 Optical Society of America

OCIS codes: (120.3930) Metrological instrumentation; (250.0250) Optoelectronics; (320.2250) Femtosecond phenomena; (320.7100) Ultrafast measurements.
http://dx.doi.org/10.1364/OL.40.000260

High bandwidth sampling is of great metrological importance in both fundamental research and industry [1]. For bandwidths from the terahertz up to the mid-infrared range, photoconducting antennas and electro-optic sampling have been employed, with both techniques having demonstrated the sampling of waveforms in the frequency range up to 40 THz [2–4]. A technique based on high harmonic generation was recently shown to provide petahertz bandwidth for sampling optical signals [5]. Here, we demonstrate a qualitatively different technique, using field emission from a sharp metal tip to directly sample an electronic signal.

In this experiment, we measure the instantaneous voltage applied to a field emission tip by mapping this voltage onto the energy of an electron. The voltage is sampled at a specific time by a femtosecond-timescale laser pulse, which triggers electron emission from the tip [6]. As the electric field from a sharp tip (~120 nm radius of curvature at the apex) decays over a short length, the voltage applied to the tip is effectively instantaneously sampled for the frequencies at which we operate [7]. The energy of the electron is then measured with the aid of a retarding grid in front of an electron detector (a microchannel plate). Thus, the laser pulse probes the voltage waveform at the tip, creating a sampling oscilloscope trace. It has been shown [8–10] that in the regime of strong field emission, this probe can exhibit sub-femtosecond features.

Conversely, if a known voltage sweep is applied to the tip, time is mapped to voltage and we can, in principle, measure the laser intensity as a function of time. This technique can also be used to lock the radio frequency (RF) phase to the repetition rate of the laser or vice versa, if both the RF waveform and the laser pulse shape are known.

The detailed experimental setup is shown in Fig. 1. Sub-10 fs pulses from a Titanium:sapphire oscillator are used to trigger emission from a tungsten field emission tip [11]. The retarding grid analyzer measures the component of the kinetic energy parallel to the tip axis. The electron beam is collimated to obtain a measured energy distribution with a width of around 2 eV (FWHM) for average tip bias voltages of 20–50 V. As proof of principle, the RF signal to be measured is derived from the harmonics of the laser repetition frequency ($f_{\mathrm{rep}} \approx 150$ MHz), which is measured with a fast photodiode. Conceptually, this is similar to a two-color pump–probe measurement, where the "pump" is the RF signal and the "probe" is the Ti:sapph laser. Delay is introduced electronically in the pump (RF), rather than optically in the probe. In a more general implementation, f_{rep} could instead be locked to the periodic signal being investigated, or to one of its subharmonics.

We measure two waveforms with the apparatus, a sine wave at 9.28 GHz and an "arbitrary" (i.e., nonsinusoidal) waveform with a fundamental at 750 MHz. A direct digital synthesizer (DDS) acts as a programmable phase shift for a signal at the frequency f_{rep} (also derived from the Ti:sapph oscillator). For the 9.28 GHz measurement, the signal is mixed with the 61st harmonic of f_{rep} to yield a signal at $62 f_{\mathrm{rep}} \approx 9.28$ GHz with programmable phase. A broadband bias tee combines this RF signal with a DC tip bias voltage. Electrical connection to the tip is made through a semirigid coaxial cable with the shield grounded at the vacuum feedthrough. Alternately, the signal from the DDS is mixed with a harmonic of f_{rep} to yield a signal near 750 Mhz and passed through a nonlinear transmission line (NLTL) to generate the "arbitrary" waveform.

Figure 2 shows the measurement at 9.28 GHz. The oscilloscope trace is obtained by stepping the phase of the RF signal and measuring the electron energy spectra with the RF alternately on and off. The difference between the center voltages of the spectra with the RF on and off reflect the voltage due to the RF signal at the time the electrons were emitted. Each voltage datum, consisting of two

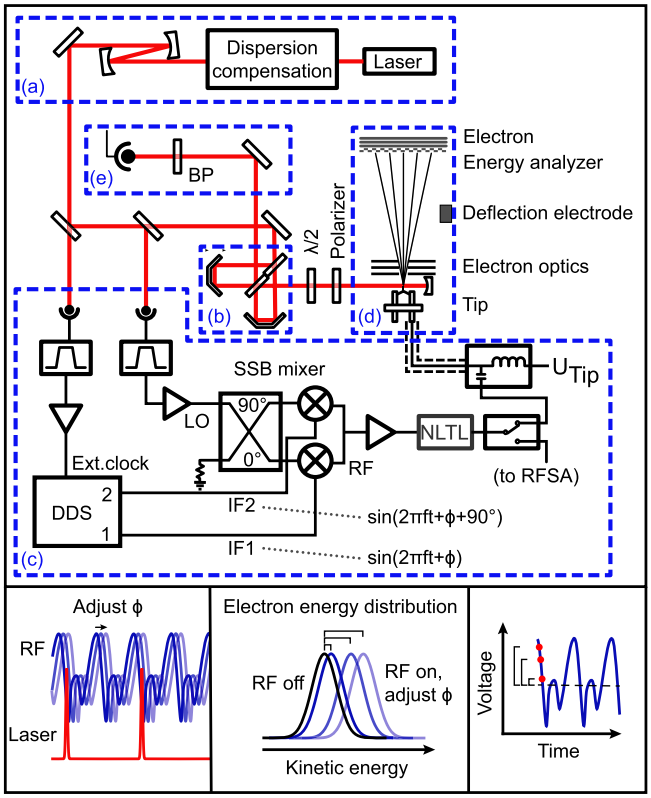

Fig. 1. (Top) Experimental setup. (a) Laser and dispersion compensation. (b) Michelson interferometer for generating multiple pulses (one arm is blocked for "oscilloscope" traces). (c) RF electronics: harmonic of laser $f_{LO} = nf_{rep}$ is mixed with DDS signal (for phase control) in a single-sideband mixer where the upper sideband is amplified and optionally put through an NLTL. For sine wave measurements, $f_{LO} = 61f_{rep} \approx 9.13$ GHz, and for NLTL measurements, $f_{LO} = 4f_{rep} \approx 600$ MHz. The signal is switched to the RF spectrum analyzer (RFSA) when no RF is applied to the tip. (d) Emitter (tip), electron optics, and energy analyzer. (e) Beam diagnostics. (Bottom) Sampling method: the phase of RF is adjusted and the energy of the emitted electrons is measured. In this way, the voltage versus time information is obtained.

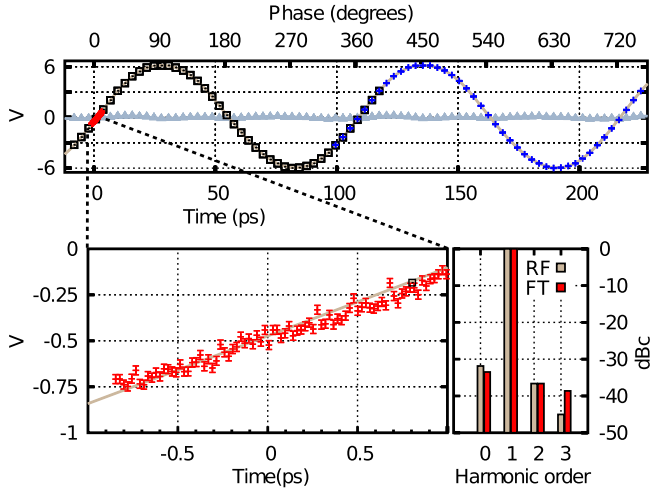

Fig. 2. Top plot shows the measured oscilloscope trace for a 9.28 GHz sine wave ($62f_{rep}$) applied to the tip. The data set (squares) is plotted again with a 360° phase offset (crosses). The plot on the lower left is a zoomed-in portion of the oscilloscope trace, with phase steps of 0.075° (22.4 fs). The plot on the lower right shows the Fourier spectrum (FT) computed from the oscilloscope trace alongside the corresponding RF amplitudes applied to the tip (at f_{LO}, $f_{LO} + f_{rep}$, $f_{LO} + 2f_{rep}$, and $f_{LO} - 3f_{rep}$). The RF spectrum was measured before the bias tee, and then corrected for the frequency response of the tip and bias tee, which was independently measured.

electron energy spectra, takes ≈200 s to measure. The statistical uncertainty in determining the voltage is calculated from the standard deviation of the electron energy spectra measured with no RF, σ_{noRF}. (A linear fit to the drift is subtracted.) As we measure the change in electron energy, the statistical uncertainty is $\sqrt{2}\sigma_{noRF} = 28$ mV for the data in Fig. 2, corresponding to a signal-to-noise ratio (SNR) of over 43 dB for the 12 Vpp 9.28 GHz sine wave. The phase noise in the RF electronics for amplification and phase control corresponds to a timing jitter of ~47 fs from 1 Hz to 100 kHz; however, timing jitter due to phase noise from the DDS and associated amplifiers could be mitigated by operating at higher frequencies. Data are measured for increasing phase, and the full data set (squares) is reproduced with a 360° offset (crosses); the overlap demonstrates the stability of the measurement. The lower left-hand plot shows a zoomed-in portion of the oscilloscope trace, with phase steps of 0.075°, corresponding to 22.4 fs.

There are some imperfections in the sine wave; namely, a small DC offset and higher order components to the Fourier spectrum. These are due to spurious mixer products, the phases of which increase by $n\phi$ as the phase ϕ of the 9.28 GHz signal is adjusted. The Fourier spectrum of the measured trace is shown in the lower right-hand plot. The $n = 0$ component is the equivalent power, due to a sine wave with the amplitude of the DC offset of the trace. For comparison, the RF amplitudes of the corresponding mixer products are plotted alongside the Fourier spectrum of the trace. The $n = 0$ component is due to the local oscillator (f_{LO}), and the $n = 2$ and $n = -3$ components are due to $f_{LO} + 2f_{rep}$ and $f_{LO} - 3f_{rep}$, respectively.

Figure 3 shows the "arbitrary" waveform generated in an NLTL. The NLTL generates a comb-like RF spectrum of the harmonics of the 750 MHz input (which is itself a harmonic of f_{rep}).

The experimental concept can be turned around: rather than detecting an unknown RF signal, one can use a known RF signal on the tip to read out amplitude-modulated optical signals. The time resolution for such a scheme is ultimately limited by the temporal response of electron emission to the laser pulse, which can follow either the intensity profile of the laser or even, in the strong-field limit, the electric field of the laser pulse [12,13].

To illustrate the concept, a Michelson interferometer is used to generate a copy of the pulse train offset in time by ~5 ps. Spectra with the double and single pulse trains were measured near the zero-crossings of the RF and are shown in Fig. 4. The highest RF streaking slope is 0.4 V/ps, obtained with the 9.28 GHz signal. From the statistical uncertainty in determining the voltage of 28 mV, the statistical uncertainty in timing at the zero-crossing is 28 mV/(0.4 V/ps) = 70 fs.

The spectra are fitted with one or two asymmetric Gaussians, to determine their relative emission times

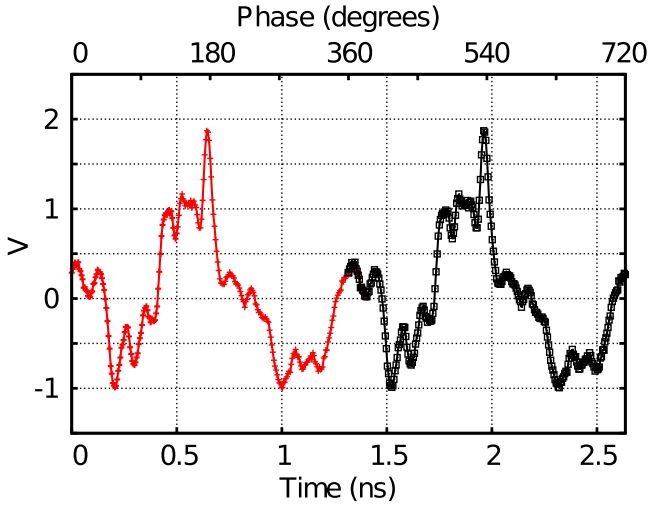

Fig. 3. NLTL oscilloscope trace representing an "arbitrary" waveform (i.e., a signal with complicated Fourier spectrum). The data set (crosses) is plotted again with a 360° offset (squares) to demonstrate stability.

(the width and skew were constrained to be the same for the double pulse spectra as for the single pulse spectra). There is some uncertainty (on the order of 100 fs) in the position of the peaks, due to line pulling from the background (e.g., secondary and scattered electrons), which was crudely modeled as an additional Gaussian peak. This is manifested as a difference in the time-delay inferred at the two zero-crossings (4.85 ps and 4.75 ps for the positive and negative slopes, respectively) and a spurious shift of the component of the spectrum due to the second pulse (solid red curve) between the top and middle plots. This shift is larger for the positive zero-crossing, where the peaks in question are closer to the background "peak" (see the bottom panel of Fig. 4).

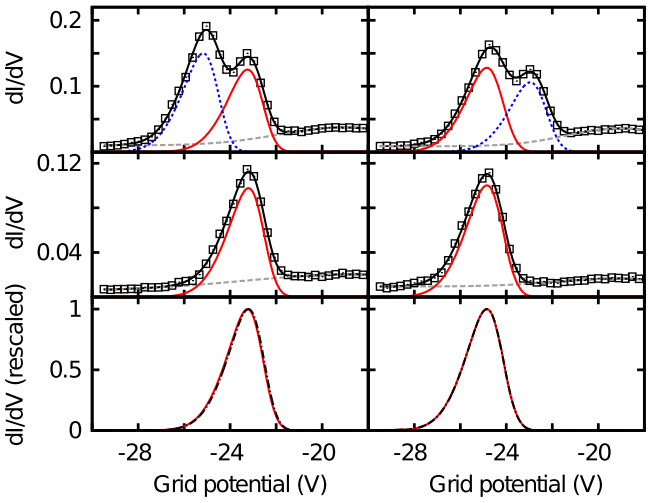

Fig. 4. Spectra with a single or double pulse train incident on the tip near a zero-crossing of the RF. The plots on the left are for the positive slope (applied voltage increases with time), and those on right are for the negative slope. (Top) Spectra for the double pulse train. (Middle) Spectra with the first pulse blocked. The spectra are fit with asymmetric Gaussians (for the main peaks, which are represented by the solid red and dotted blue lines), and the background from the secondary and scattered electrons is fitted with a Gaussian (gray dashed line). The total fits are shown as solid black lines through the data points. (Bottom) The plots show the red curves from the top and middle plots, normalized to their peak values (the solid red line represents the double pulse spectra and black dashed–dotted line represents the single pulse spectra). The difference in position between the two fits corresponds to 110 fs for the positive slope and 10 fs for the negative slope.

Both the RF waveform and laser intensity sampling techniques could be advanced further by increasing the energy resolution of the analyzer. State-of-the-art energy spectrometers easily achieve an energy resolution in the milli-electron volts range and could allow faster, parallel readout of the spectra [14,15]. The resolution will then be limited by the initial energy spread of the emitted electrons, which is on the order of 0.5 eV for ultrafast laser-induced emission from the metal nanotips [16].

Better energy resolution and accuracy in the few femtosecond range could also be obtained by increasing the slope of voltage versus time at the RF zero-crossing. One approach to accomplishing this would be to use a microwave cavity to build up strong fields [17]. In such a scheme, the emission tip could be placed directly inside the microwave cavity. Numerical simulations using realistic geometries [18] and RF power suggest that the streaking of 40 mV/fs is realizable, an improvement of two orders of magnitude over our current setup. Such an optimized setup would enable the measurement of the RF phase with respect to the femtosecond laser pulses with ~10 fs accuracy upon the energy-resolved detection of a single electron.

To summarize, ultrafast laser-triggered electron emission from a metal nanotip is used to construct an oscilloscope, which records an RF waveform with the temporal resolution tied to the temporal width of the laser pulses with an accuracy of 28 mV. The laser intensity as a function of time is also probed, demonstrating the ability to discern two consecutive laser pulses separated by 5 ps.

This research is funded by the Gordon and Betty Moore Foundation, and by work supported under the Stanford Graduate Fellowship.

References

1. F. Krausz and M. I. Stockman, Nat. Photonics **8**, 205 (2014).
2. S. Kono, M. Tani, and K. Sakai, Appl. Phys. Lett. **79**, 898 (2001).
3. P. Gaal, M. B. Raschke, K. Reimann, and M. Woerner, Nat. Photonics **1**, 577 (2007).
4. G. Ghione, *Semiconductor Devices for High-Speed Optoelectronics*, 1st ed. (Cambridge University, 2009).
5. K. T. Kim, C. Zhang, A. D. Shiner, B. E. Schmidt, F. Légaré, D. M. Villeneuve, and P. B. Corkum, Nat. Photonics **7**, 958 (2013).
6. P. Hommelhoff, C. Kealhofer, A. Aghajani-Talesh, Y. R. Sortais, S. M. Foreman, and M. A. Kasevich, Ultramicroscopy **109**, 423 (2009).
7. L. Wimmer, G. Herink, D. R. Solli, S. V. Yalunin, K. E. Echternkamp, and C. Ropers, Nat. Phys. **10**, 432 (2014).
8. M. Krüger, M. Schenk, and P. Hommelhoff, Nature **475**, 78 (2011).

9. G. Herink, D. R. Solli, M. Gulde, and C. Ropers, Nature **483**, 190 (2012).
10. B. Piglosiewicz, S. Schmidt, D. J. Park, J. Vogelsang, P. Groß, C. Manzoni, P. Farinello, G. Cerullo, and C. Lienau, Nat. Photonics **8**, 37 (2013).
11. P. Hommelhoff, Y. Sortais, A. Aghajani-Talesh, and M. A. Kasevich, Phys. Rev. Lett. **96**, 077401 (2006).
12. P. Hommelhoff, C. Kealhofer, and M. A. Kasevich, Phys. Rev. Lett. **97**, 247402 (2006).
13. M. Schenk, M. Krüger, and P. Hommelhoff, Phys. Rev. Lett. **105**, 257601 (2010).
14. M. Yavor, *Optics of Charged Particle Analyzers* (Academic, 2009).
15. M. Terauchi, M. Tanaka, K. Tsuno, and M. Ishida, J. Microsc. **194**, 203 (1999).
16. H. Yanagisawa, M. Hengsberger, D. Leuenberger, M. Klöckner, C. Hafner, T. Greber, and J. Osterwalder, Phys. Rev. Lett. **107**, 087601 (2011).
17. A. Gliserin, A. Apolonski, F. Krausz, and P. Baum, New J. Phys. **14**, 073055 (2012).
18. A. Williamson, IEEE Trans. Microwave Theor. Tech. **24**, 182 (1976).